Progress In Electromagnetics Research, Vol. 138, 83–98, 2013

ON THE USE OF IMPROVED IMAGING TECHNIQUES FOR THE DEVELOPMENT OF A MULTISTATIC THREE-DIMENSIONAL MILLIMETER-WAVE PORTAL FOR PERSONNEL SCREENING

Borja Gonzalez-Valdes[1, *], Yuri Álvarez[2], José Á. Martínez[1], Fernando Las-Heras[2], and Carey M. Rappaport[1]

[1]The Gordon CenSSIS/ALERT Center of Excellence, Northeastern University, Boston, MA 02115, USA

[2]Department of Electrical Engineering, Universidad de Oviedo, Campus Universitario, Gijón, Asturias 33203, Spain

Abstract—The design and evaluation of an active three dimensional (3D) millimeter wave imaging system for personnel security screening is presented in this work. The system is able to produce a high-resolution 3D reconstruction of the whole human body surface and reveal concealed objects under clothing. Innovative multistatic millimeter wave radar designs and algorithms, which have been previously validated, are combined to significantly improve the previous reconstruction results. In addition, the system makes use of a reduced amount of information, thus simplifying portal design. Representative simulation results showing good performance of the proposed system are provided and supported by sample measurements.

1. INTRODUCTION

Imaging techniques based on electromagnetic waves are used in a wide range of systems [1–6] for security and medical applications. In the area of homeland security, there is an increasing demand for methods which will improve the efficiency of the personnel screening at security checkpoints for concealed objects and for contraband detection. Human body imaging is an effective means of identifying dangerous objects attached to the body under clothing [3–6]. Terahertz wave sensing [7, 8] and X-ray radar [9] provide good resolution, but the former is based on expensive, cutting-edge technology and relies on

Received 14 February 2013, Accepted 4 March 2013, Scheduled 16 March 2013

* Corresponding author: Borja Gonzalez-Valdes (b.gonzalezvaldes@neu.edu).

mechanical scanning for its speed and accuracy, while the X-ray based systems make use of ionizing emissions.

Active nearfield millimeter-wave imaging radar systems are very good candidates for achieving high-resolution imaging, while also balancing the trade-off between accuracy and cost. With mm-wave radar, the object of interest is first illuminated by millimeter waves and then the scattered field is measured and processed in order to reconstruct the surface (or volume) of the object. The image resolution is determined by the radar center frequency, its bandwidth, and its aperture size. Since some concealed objects may have distinguishing features as small as 1 cm, a system providing at least this resolution is required for good object discrimination.

Current state of the art millimeter wave portal imaging systems [3] are based on monostatic radar and Fourier inversion [10]. These systems are inherently fast, but present disadvantages of reconstruction artifacts such as dihedral effects and misrepresenting sudden indentations and protrusions due to the monostatic nature of the collected electric field data.

More advanced techniques for the reconstruction of surface induced currents and shape reconstruction exist. One possibility is based on contour parameterization [11, 12]. Other techniques are based on the so-called inverse source problem [13, 14], where a set of equivalent currents are reconstructed within a domain that encloses the object(s)-under-test. These inverse source methods can be accelerated using the Fast Multipole Method (FMM) [15, 16].

This work presents the design and evaluation of a new millimeter-wave based portal system able to generate three-dimensional high-resolution images of the whole human body. In a previous work, the idea of 3D reconstruction using 2D stacked SAR images has been presented [17], together with the use of fast multistatic Synthetic Radar Aperture (SAR) imaging [16]. The new contributions of this work are: i) The use of a limited number of observation points. While [17], required a cylindrical observation domain, this contribution proposes the use of 2 arrays of receivers vertically displaced. ii) The use of an improved imaging technique that refines the contour estimation [18], which also avoids the need of a lower frequency band as in [17], thus simplifying the design of the proposed mm-wave portal based imaging system. iii) Experimental validation of the proposed techniques.

This paper is structured as follows: Section 2 describes the proposed imaging system configuration, highlighting the use of the Blade Beam reflector antenna and a limited number of receivers. An overview of the imaging algorithms is presented in Section 3. Section 4 shows simulation results, proving that the novel contributions allow

an accurate profile reconstruction of the human body torso. Finally, validation of the techniques with measurements for a 2D case is presented in Section 5.

2. IMAGING SYSTEM AND CONFIGURATION

2.1. Portal Setup

The general configuration of the proposed system is shown in Figure 1. The body is illuminated by an incident millimeter-wave beam which is generated by a novel elliptical-parabolic reflector antenna which generates a narrow beam in elevation (z axis) while illuminating the body with constant amplitude in azimuth [19]. This illumination allows thin slices (2–3 cm thickness) of the body to be processed independently. The field scattered by the section under illumination is captured by two arrays of millimeter wave antenna elements placed on a 90 degree arc above and below the reflector. An advanced imaging algorithm described in Section 3 is used to transform the scattered field information into a reconstruction of one slice of the human body (with any objects placed on it) with constant height along z axis. The reflector and receiving antenna arrays are translated vertically, and the two-dimensional retrieved images are stacked to form a full body surface reconstruction. This approach simplifies the three-dimensional reconstruction problem into a combination of multiple 2D problems which ultimately reduces the computational cost

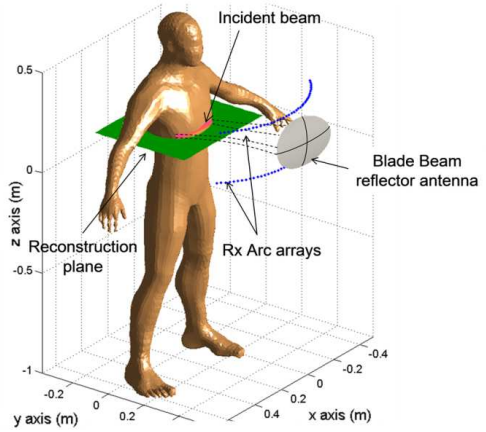

Figure 1. Geometry of the proposed measurement setup for human body imaging by using millimeter waves.

and thus the processing time of the full 3D inversion problem (up to two orders of magnitude with respect to [17]), an essential requirement for practical security screening systems.

2.2. Blade Beam Reflector Antenna

To generate a line focus at a medium distance (∼0.5 m), a new type of reflector is proposed. It combines the spot focusing in the vertical plane with collimation in the horizontal direction. The reflector is thus a blending of elliptical curvature in height with parabolic in width [19]. As a reflector antenna, it is inherently broadband, relatively light, and easy to characterize.

Figure 2 shows the 60.5 GHz field generated by the reflector by using Physical Optics (PO) and as measured with a field sampling probe, as a function of vertical position, in the focal region, 60 cm in front of the reflector. There is reasonable agreement between the measured and modeled patterns in the secondary focal region, demonstrating focusing in the vertical plane. From 56–64 GHz, the −3 dB beamwidth is about 1 cm, which allows for the interrogation and reconstruction of just a narrow vertical portion of the target object. A photograph of the fabricated reflector antenna is also displayed in Figure 2.

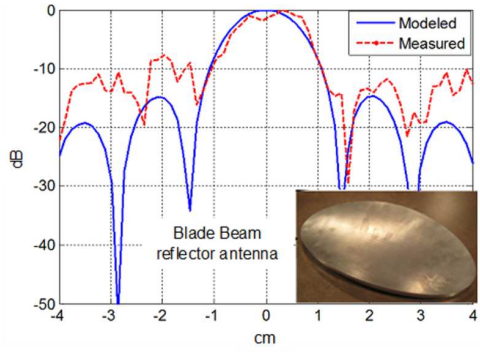

Figure 2. Modeled and measured antenna pattern in the elevation plane (f = 60.5 GHz) and photograph of the fabricated Blade Beam reflector.

3. OVERVIEW OF THE IMAGING TECHNIQUES

3.1. Inverse Fast Multipole Method (iFMM)

The image of each slice of the body illuminated through the reflector antenna is created by using the inverse Fast Multipole Method

(iFMM) [16]. This method is based on the multipolar expansion of the electromagnetic field integral equation relating the scattered fields $\vec{E}(\vec{r})$ to a set of electric currents $\vec{J}(\vec{r})$ defined on a surface V' that radiate the same fields as the original set of metallic scatterers (see Eq. (1) in [15]). The underlying method of the FMM is to divide the radiated field domain and the current domain into several groups, so that only the interactions between these groups are calculated, thus reducing the number of operations to be done. One of the advantages of the FMM when applied to inverse problems is that the observation and source domains are physically different, so in most cases, there are no adjacent groups. Furthermore, if the distance between the observation and source domains is large enough, then the FMM far-field condition [15] is satisfied for all the groups, allowing translation matrix simplification.

The FMM can also be applied to the inverse scattering problem. Thus, the electric currents can be calculated from the scattered fields. The described multipolar expansion uses a plane wave operator for aggregation on the sources domains and disaggregation on the reconstruction domain, while the far field translation operator is the free-space spherical propagation term. In the case of the inverse problem, these operations are inverted as indicated in [16] so the inverse problem is solved in a forward fashion. The obtained iFMM images are similar to those generated by conventional SAR (Synthetic Aperture Radar) processing [16].

3.2. Virtual Focusing Concept

The SAR image obtained using the iFMM provides a good approach to the position and shape of the body contour. However, depending on the available bandwidth of the radar system, it is proposed a novel imaging technique to improve the system resolution from the same scattered field data used to build the SAR image.

Taking into account the reciprocity theorem and array theory [18], the backpropagated field, $\vec{E}_u^f$, on the image region centered at $\vec{\rho'}_u$ for a frequency f can be calculated as (Figure 3):

$$\vec{E}_u^f(\vec{\rho'}_u) \propto \sum_p \vec{E}_{scatt}^f(\vec{\rho}_p) e^{+jk_0^f R(\vec{\rho}_p, \vec{\rho'}_u)} \tag{1}$$

where $\vec{E}_{scatt}^f(\vec{\rho}_p)$ is the field observed by an antenna located at $\vec{\rho}_p$ at frequency f and $R(\vec{\rho}_p, \vec{\rho'}_u)$ is the distance from $\vec{\rho}_p$ to $\vec{\rho'}_u$. The Point Spread Function (PSF) derived from the backpropagation of the field $\vec{E}_u^f$ will depend on the size of the observation arc: the wider the

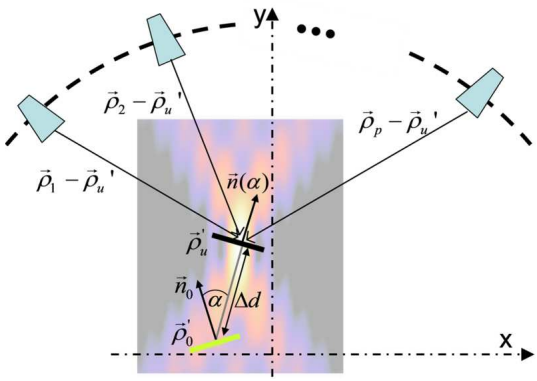

Figure 3. Virtual focusing idea. Top view of the geometry configuration and vector notation. Background: amplitude of the beam generated using the phase law on the p-receivers to focus on the targeted position.

observation arc, the narrower the PSF in cross-range (x-axis), thus allowing for the consideration of smaller isolated sections.

By using this approach it is possible to optimize different sections of the contour found from the SAR image so that the pixel by pixel difference of the backpropagated fields is minimized. The method consists of focusing the field on each of the facets in which the contour derived from the image is discretized. Next, for each retrieved facet, placed originally at $\vec{\rho'}_0$, the following cost function F is optimized (2), so that the minimum will correspond to the position and orientation corresponding to the true profile.

$$F(\Delta d, \Delta\alpha) = \sum_f \frac{\left| \vec{E}^f_u - \sum_p \vec{E}^f_{facet}(\Delta d, \Delta\alpha) e^{+jk_0^f R(\vec{\rho}_p, \vec{\rho'}_u)} \right|}{\left| \vec{E}^f_u \right|} \quad (2)$$

where $\sum_p \vec{E}^f_{facet}(\Delta d, \Delta\alpha) e^{+jk_0^f R(\vec{\rho}_p, \vec{\rho'}_u)}$ represents the simulated back-propagated field of a test facet that has been moved from its original position $\vec{\rho'}_0$ to a point $\vec{\rho'}_u = \vec{\rho'}_0 + \Delta\vec{\rho'}$ where $\Delta\vec{\rho'} = \Delta d[(\hat{n}_{0x}\cos(\Delta\alpha) + \hat{n}_{0y}\sin(\Delta\alpha))\hat{x} + (\hat{n}_{0y}\cos(\Delta\alpha) - \hat{n}_{0x}\sin(\Delta\alpha))\hat{y}]$. $\Delta\alpha$ is the angle between the normal of the facet and the line along which the facet position is swept and Δd is the length of the line along that the facet position is tested. Figure 3 shows the vector notation relating one point of the reconstruction domain to the receiving positions in the semi-cylindrical domain where the field is measured.

The virtual focusing estimates the right position and the orientation of an isolated facet $\vec{\rho'}_u$, starting from an initial guess $\vec{\rho'}_0$ which is typically derived from the SAR image amplitude. However, a better first guess can be obtained if the SAR image phase is used as well. The underlying principle is that the SAR image phasefronts are related to the shape of the object contour (see Figures 8(b) and 11(b) for a better understanding of the SAR image phasefronts behavior). However, it is not possible to determine which phasefront is the one matching the true profile. Thus, the proposed idea is to select those phasefronts corresponding to to SAR image reflectivity values having an amplitude $> -10\,\text{dB}$ below the SAR image amplitude maximum. Next, these phasefronts are discretized into facets, which will be used as the first guess for the virtual focusing technique. The main advantage is that the phasefronts provide the correct orientation of the facet, $\Delta\alpha$, so only the position of the facet needs be optimized. That is the cost function (2) is minimized only as a function of Δd [18].

The virtual focusing technique uses the same scattered field information collected for the SAR image retrieval, avoiding the need to measure at different frequency reference as proposed in [17].

4. SETUP EVALUATION

Having defined the proposed mm-wave portal based imaging physical configuration and reconstruction algorithms, the next step is to simulate its performance. The field scattered by the modeled human body torso is calculated using Physical Optics (PO). A full wave Method of Moments method could have been used, but PO is sufficiently accurate and much faster at computing scattering from large, smooth scatterers.

As mentioned in a prior report [17], the first approach is to observe the scattered field across a large densely sampled cylindrical domain. However, for this particular body scanning application it is very important to achieve the reconstruction with a much more limited number of observation points in order to decrease the system cost and acquisition and processing times.

Figure 4 shows a section of the illuminated torso and the field that the body scatters in a cylindrical observation domain discretized into 10201 observation points [17]. The position of two observation arcs with 201 observation points in each 0.75 m radius arc is also plotted. The incident field, generated by the Blade Beam reflector antenna on the human body, can be described as a converging cylindrical wave that is mostly polarized in the z-direction.

Figure 5(a) shows the 2D slice reconstructed image when the

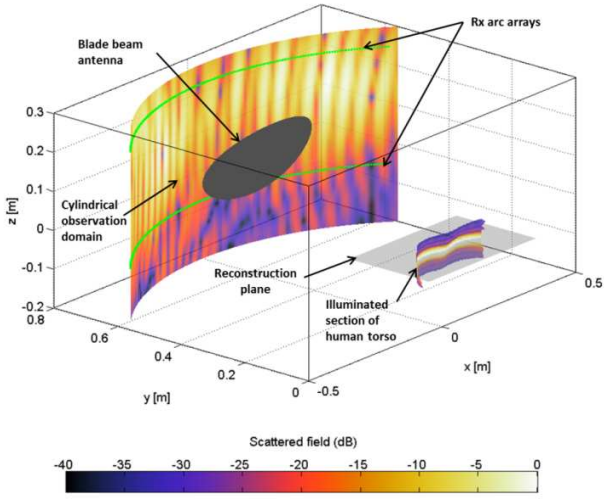

Figure 4. Scattered field on an observation cylinder when a section of the human body is illuminated by the Blade Beam antenna. Position of the observation arcs is also plotted.

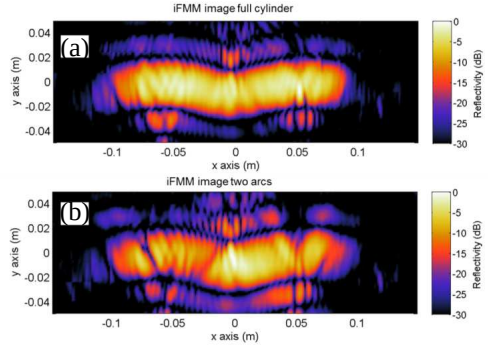

Figure 5. Reconstructed SAR image (normalized amplitude, dB) for z-polarized fields. Plane $z = 2\,\text{cm}$. Observation domain. (a) Full cylinder. (b) Two observation arcs.

incident beam is illuminating the body at $z = 2\,\text{cm}$ above the central torso plane. In this case, all of the scattered field information on the entire cylindrical observation domain is used. Figure 5(b) presents the same 2D slice reconstruction when only the two 90 degree arcs are used as the observation points. The working frequency band is taken from 60 to 66 GHz, in 600 MHz-steps (resulting in 11 frequencies). The results of the two inversions are comparable since the antenna illumination

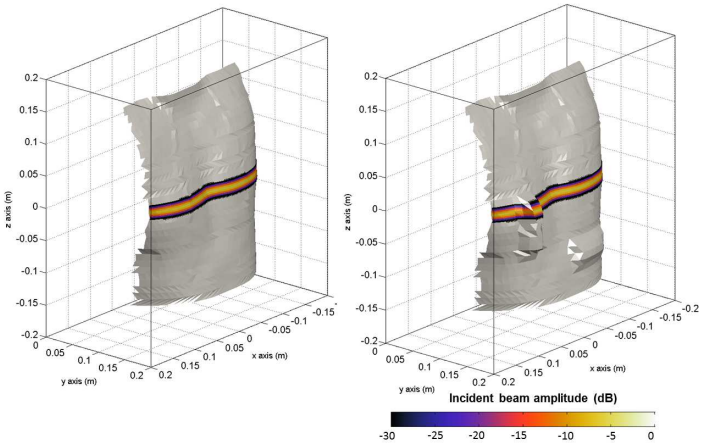

Figure 6. Human body torso model and incident field amplitude distribution when the beam is pointing at $z = 0\,\mathrm{m}$. (a) Original human body torso. (b) Human body torso with two objects placed on top.

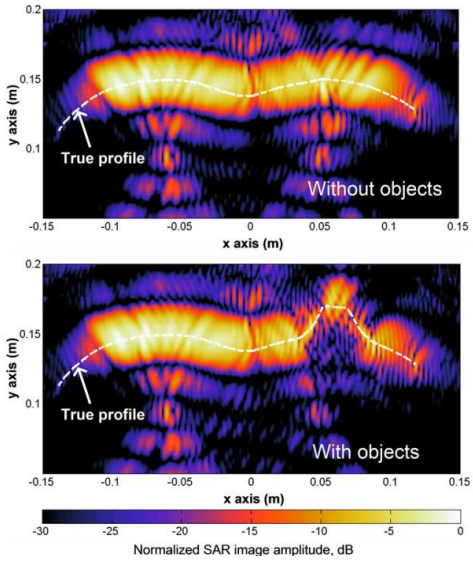

Figure 7. Retrieved SAR image (normalized amplitude, dB) on the slice $z = 0\,\mathrm{m}$. Upper plot: human body torso with no objects. Lower plot: the slice intersects one of the objects placed on the torso, as indicated by dashed white curve.

reduces the three-dimensional problem to a two-dimensional one. The savings in computational cost for solving this simplified inverse problem is about two orders of magnitude. The reduction of observation points with respect to [17] and the use of the iFMM make the system suitable for real-time image calculation, as each SAR image is calculated in 2 s on a conventional laptop.

Figure 6 shows a model of the human torso illuminated by the Blade Beam antenna at 63 GHz when the beam is pointing at $z = 0$ m. Cases with and without two metallic objects placed on the body surface are depicted. Even when the human body contour with and without concealed objects (e.g., Figure 7) can be clearly identified by observing the highest amplitude values, the development of an automatic image processing method that is able to extract the exact contour is a challenging image-processing task. A simple algorithm to address this issue based on the choice of the highest amplitude value on y-axis for a given x-axis coordinate is proposed. Good agreement between the true

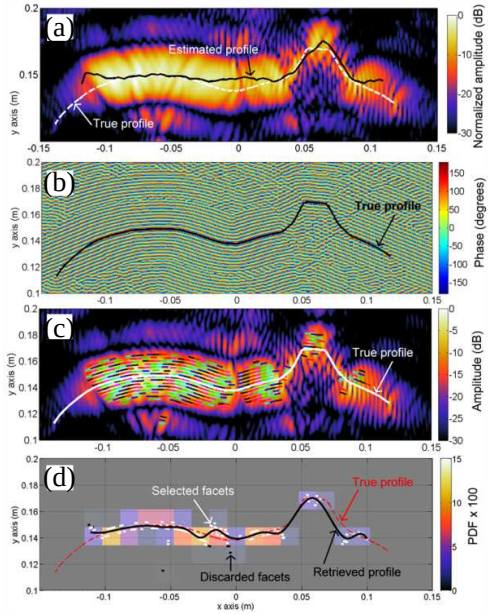

Figure 8. (a) SAR image of the $z = 0$ body slice. Amplitude and contour extraction (solid black line). (b) Phase, in degrees. (c) Facets corresponding to the segmented phase fronts, plotted on top of the SAR image amplitude. (d) Optimized facets, showing which are selected (white segments) and discarded (black segments) according to a PDF criterion of 0.02. Solid black line represents the final retrieved profile.

human body torso with object (dashed white line) and the retrieved profile (solid black line) can be observed in Figure 8(a).

The next step is the application of the improved imaging technique based on the virtual focusing concept (Section 3.2). From the SAR image phase (Figure 8(b)), it is observed that the phase fronts are parallel to the original profile. Several phase fronts are extracted from the image phase using the image amplitude to segment the phase fronts in 400 facets (Figure 8(c)), then applying the virtual focusing method to estimate the position of the facets.

Further improvement can be made by eliminating those facets whose positions are incorrectly estimated (black segments in Figure 8(d)). To do this, the area where the SAR image is retrieved is divided into subdomains of $\Delta S = (1.5\lambda)^2$ at 60 GHz. The number of facets lying on each subdomain is then evaluated, obtaining a probability density function (PDF) that provides information about the number of facets per subdomain. Only the facets belonging to high-PDF subdomains are considered for final profile estimation.

The previous methodology is illustrated in Figure 8(d), where the PDF associated to each subdomain is also plotted. Facets are selected according to a PDF = 0.02 criterion. The selected facets, plotted in white, are used to generate a curve (black solid line), which clearly fits the true profile: the Root Mean Square error (RMSE) between the true profile and this curve is less than 5 mm.

The retrieved contour lines for every slice are stacked to create a three-dimensional mesh. Ten retrieved contour lines (from $z = -12$ cm

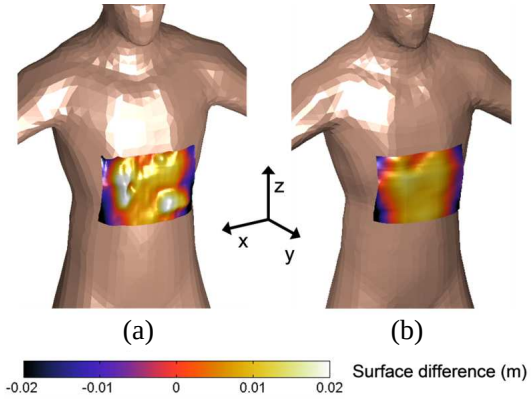

Figure 9. Detection capabilities using the 3D meshes from the stacked 2D contour retrieved on every slice. (a) Two objects are placed on the human body torso. (b) No objects on torso.

to $z = 6\,\text{cm}$, in 2 cm steps) are combined in order to obtain the 3D surface that approaches the true human body profile. The resulting meshes for the case of the body with and without objects are generated and processed as indicated in [17] to produce a smooth surface used as a reference. Thus, the retrieved 3D mesh is compared to the smoothed 3D mesh so that sharp variations expected to correspond with the presence of concealed objects can be detected. Figure 9 shows the detection capabilities provided by the described setup. If compared to Figure 10 of [17], the detection capabilities are clearly kept.

5. VALIDATION WITH MEASUREMENTS

In order to validate the simulation results, a set of experimental measurements has been performed. Since the 60 GHz final configuration using the Blade Beam reflector antenna is still under development and testing, preliminary lower frequency measurements using the metallic torso model shown in Figure 10 have been performed.

The target is a bent metallic surface that aims to model the human body torso curvature. A 2.5 cm thick metallic object (wood covered with aluminum foil) is placed vertically, at the front. The

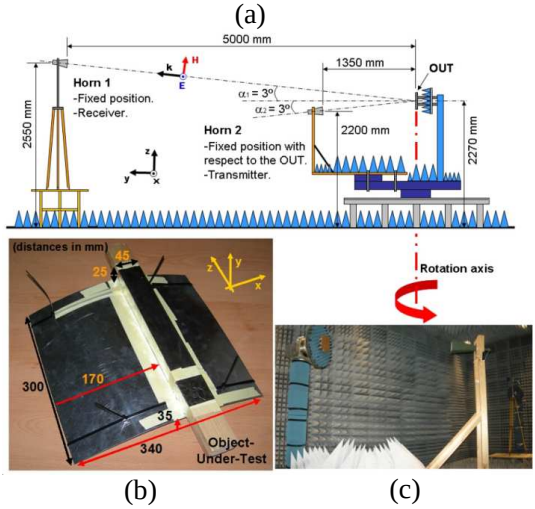

Figure 10. (a) SAR measurement setup scheme. (b) Metallic curved torso-mimicking surface object-under-testwhich has z axis invariant geometry. (c) Measurement setup at the spherical range in anechoic chamber.

geometry is illuminated using a horn placed at 1.35 m (denoted as Horn 2 in Figure 10), to simulate quasi-planar illumination of the body. Thus, over the region of interest, the geometry and the illumination are both independent of vertical position, which models the Blade Beam illumination. The frequency range is 18 to 26 GHz, in 500 MHz-steps. The field scattered by the metallic target has been measured on a 180 degrees arc placed 5 m away of the object. In this case, the measurement setup (also depicted in Figure 10) does not allow displacement along z axis, so the SAR image is recovered in only one slice. The retrieved image and the estimated object contour derived for this experiment are shown in Figure 11(a). It is clear, observing the agreement between the recovered and true profile, that the maximum amplitude points can be used to identify the shape of the object under test. Following the same procedure described in the previous section, the improved imaging method is applied to these measured data. The SAR image phase is plotted in Figure 11(b), showing the fitting between the true metallic profile and the phasefronts. Figure 11(c) presents the reconstructed profile, together with the true profile, the PDF function, and the optimized facets (discarded and selected

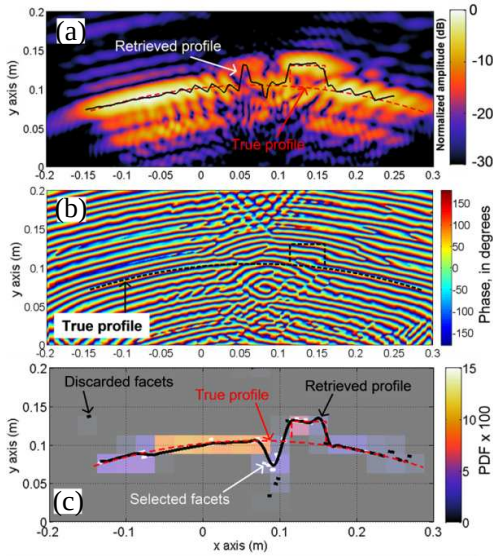

Figure 11. (a) SAR image from measured data using the iFMM and extracted contour using the maximum amplitude values. (b) Phase of the SAR image. (c) PDF plot, selected and discarded facets, true profile, and final retrieved profile using the proposed method.

ones according to a PDF criterion of 0.01). Again, the retrieved profile fits the true profile better than in the amplitude-only results (Figure 11(a)).

6. CONCLUSIONS

A new design for a three-dimensional millimeter-wave portal-based imaging system for personnel inspection has been presented. Based on the simulation and experimental results, the system will be able to generate real time, high resolution images of the human body surface and any objects concealed under clothing by using a limited number of observation points. The contributions are: a novel Blade Beam reflector transmitting antenna that produces narrow target illumination to allow accurate stacked 2D reconstructions of the 3D surface; a carefully positioned multistatic array receiving antenna for artifact-free imaging; the inverse FMM for improved radiating current-based SAR-like reconstruction; an improved imaging processing that uses the amplitude and phase information provided by the SAR image, and most importantly, experimental validation of the modeling and reconstruction. These improvements will lead to faster, more accurate person imaging to improve the security screening process.

ACKNOWLEDGMENT

This work is supported by CenSSIS, the Gordon Center for Subsurface Sensing and Imaging Systems NSF ERC Program (Award Number EEC-9986821); by the Ministerio de Ciencia e Innovacin of Spain/FEDER under projects CONSOLIDER-INGENIO CSD2008-00068 (TERASENSE), IPT-2011-0951-390000 (TECNIGRAF), and TEC2011-24492/TEC (iSCAT); by PCTI Asturias under projects EQUIP08-06, FC09-COF09-12, EQUIP10-31, and PC10-06 (FLEXANT). This material is based upon work supported by the Science and Tech. Directorate, U.S. Department of Homeland Security under the Award Number 2008-ST-061-ED0001.

REFERENCES

1. Li, S., B. Ren, H.-J. Sun, W. Hu, and X. Lv, "Modified wavenumber domain algorithm for three-dimensional millimeter-wave imaging," *Progress In Electromagnetics Research*, Vol. 124, 35–53, 2012.

2. Martinez-Lorenzo, J. A., C. M. Rappaport, and F. Quivira, "Physical limitations on detecting tunnels using underground-focusing spotlight synthetic aperture radar," *IEEE Transactions on Geoscience and Remote Sensing*, Vol. 49, No. 1, 65–70, Jan. 2011.
3. Sheen, D. M., D. L. McMakin, and T. E. Hall, "Three-dimensional millimeter-wave imaging for concealed weapon detection," *IEEE Transactions on Microwave Theory and Techniques*, Vol. 49, No. 9, 1581–1592, Sep. 2001.
4. Martínez-Lorenzo, J. A., F. Quivira, and C. M. Rappaport, "SAR imaging of suicide bombers wearing concealed explosive threats," *Progress In Electromagnetics Research*, Vol. 125, 255–272, 2012.
5. Angell, A. and C. Rappaport, "Computational modelling analysis of radar scattering by clothing covered arrays of metallic body-worn explosive devices," *Progress In Electromagnetics Research*, Vol. 76, 285–298, 2007.
6. Demirci, S., H. Cetinkaya, E. Yigit, C. Ozdemir, and A. A. Vertiy, "A study on millimeter-wave imaging of concealed objects: Application using back-projection algorithm," *Progress In Electromagnetics Research*, Vol. 128, 457–477, 2012.
7. Cooper, K. B., R. J. Dengler, N. Llombart, B. Thomas, G. Chattopadhyay, and P. H. Siegel, "THz imaging radar for standoff personnel screening," *IEEE Transactions on Terahertz Science and Technology*, Vol. 1, No. 1, 169–182, Sep. 2011.
8. Friederich, F., W. von Spiegel, M. Bauer, F. Meng, M. Thomson, B. Lisauskas, B. Hils, V. Krozer, A. Keil, T. Lffler, R. Henneberger, A. Huhn, G. Spickermann, P. Bolvar, and H. Roskos, "THz active imaging systems with real-time capabilities," *IEEE Transactions Terahertz Science and Technology*, Vol. 1, No. 1, 183–200, 2011.
9. Eilbert, R. F. and S. Shi, "Improved imaging for X-ray inspection systems," *IEEE Aerospace and Electronic Systems Magazine*, Vol. 20, No. 3, 23–28, 2005.
10. Lopez-Sanchez, J. and J. Fortuny-Guasch, "3-D radar imaging using range migration techniques," *IEEE Transactions on Antennas and Propagation*, Vol. 48, No. 5, 728–737, May 2000.
11. Martinez-Lorenzo, J. A., B. Gonzalez-Valdes, C. M. Rappaport, J. G. Meana, and A. G. Pino, "Reconstructing distortions on reflector antennas with the iterative-field-matrix method using near-field observation data," *IEEE Transactions on Antennas and Propagation*, Vol. 59, No. 6, 2434–2437, Jun. 2011.
12. Lin, C. Y. and Y. W. Kiang, "Inverse scattering for conductors by

the equivalent source method," *IEEE Transactions on Antennas and Propagation*, Vol. 44, No. 3, 310–316, Mar. 1996.

13. Pastorino, M., A. Massa, and S. Caorsi, "A microwave inverse scattering technique for image reconstruction based on a genetic algorithm," *IEEE Trans. Instr. and Meas.*, Vol. 49, No. 3, 573–578, Jun. 2000.
14. Álvarez, Y., B. A. Casas, C. García, and F. Las-Heras, "Geometry reconstruction of metallic bodies using the sources reconstruction method," *IEEE Ant. Wireless Prop. Letters*, Vol. 9, 1197–1200, 2009.
15. Chew, W. C., T. J. Cui, and J. M. Song, "A FAFFA-MLFMA algorithm for electromagnetic scattering," *IEEE Transactions on Antennas and Propagation*, Vol. 50, No. 11, 1640–1649, 2002.
16. Álvarez, Y., J. A. Martínez, F. Las-Heras, and C. M. Rappaport, "An inverse fast multipole method for geometry reconstruction using scattered field information," *IEEE Transactions on Antennas and Propagation*, Vol. 60, No. 7, 3351–3360, Jul. 2012.
17. Álvarez, Y., B. Gonzalez-Valdes, J. A. Martínez, F. Las-Heras, and C. M. Rappaport, "3D whole body imaging for detecting explosive-related threats," *IEEE Transactions on Antennas and Propagation*, Vol. 60, No. 9, 4453–4458, Sep. 2012.
18. Álvarez, Y., B. Gonzalez, J. A. Martínez, F. Las-Heras, and C. Rappaport, "An improved SAR based technique for accurate profile reconstruction," *IEEE Transactions on Antennas and Propagation*, Vol. PP, No. 99, 1, 2012.
19. Rappaport, C. and B. Gonzalez-Valdes, "The blade beam reflector antenna for stacked nearfield millimeter-wave imaging," *IEEE International Symposium on Antennas and Propagation*, 1–2, Chicago, Jul. 2012.